J Comput Aided Mol Des (2014) 28:779–794
DOI 10.1007/s10822-014-9771-x

Ensemble pharmacophore meets ensemble docking: a novel screening strategy for the identification of RIPK1 inhibitors

S. M. Fayaz · G. K. Rajanikant

Received: 26 February 2014 / Accepted: 23 June 2014 / Published online: 1 July 2014

Abstract Programmed cell death has been a fascinating area of research since it throws new challenges and questions in spite of the tremendous ongoing research in this field. Recently, necroptosis, a programmed form of necrotic cell death, has been implicated in many diseases including neurological disorders. Receptor interacting serine/threonine protein kinase 1 (RIPK1) is an important regulatory protein involved in the necroptosis and inhibition of this protein is essential to stop necroptotic process and eventually cell death. Current structure-based virtual screening methods involve a wide range of strategies and recently, considering the multiple protein structures for pharmacophore extraction has been emphasized as a way to improve the outcome. However, using the pharmacophoric information completely during docking is very important. Further, in such methods, using the appropriate protein structures for docking is desirable. If not, potential compound hits, obtained through pharmacophore-based screening, may not have correct ranks and scores after docking. Therefore, a comprehensive integration of different ensemble methods is essential, which may provide better virtual screening results. In this study, dual ensemble screening, a novel computational strategy was used to identify diverse and potent inhibitors against RIPK1. All the pharmacophore features present in the binding site were captured using both the apo and holo protein structures and an ensemble pharmacophore was built by combining these features. This ensemble pharmacophore was employed in pharmacophore-based screening of ZINC database. The compound hits, thus obtained, were subjected to ensemble docking. The leads acquired through docking were further validated through feature evaluation and molecular dynamics simulation.

Keywords Necroptosis · RIPK1 · Ensemble pharmacophore · Ensemble docking · Dual ensemble screening (DES)

S. M. Fayaz · G. K. Rajanikant (✉)
School of Biotechnology, National Institute of Technology Calicut, Calicut 673601, India
e-mail: rajanikant@nitc.ac.in

Introduction

Programmed cell death (PCD) is a fundamental regulatory process seen during animal development and in many diseases. Apoptosis and autophagy are well conserved, established and well-studied forms of PCD mechanism [1, 2]. Mounting evidence indicate that the cells have an alternative programmed means for cell death called programmed necrosis or necroptosis, the activation of which has been observed in diverse animal models of human pathologies such as neonatal brain hypoxia [3], acute pancreatitis [4, 5], multiple organ failure [6] and cerebral ischemia [7–9]. Necroptosis is quite distinct from apoptosis, as it does not involve key apoptosis regulators such as caspases and Bcl-2 family members, or cytochrome c release from mitochondria. The cell morphology of necroptotic death is very similar to that of necrosis, including early loss of plasma membrane integrity, lack of nuclear fragmentation, mitochondrial dysfunction and oxidative stress. It is probable that pharmacological agents targeting the molecular signalling mechanisms that control death execution pathways, such as necroptosis, may offer prospects for more effective and long-standing cellular protection in diseases involving PCD.

The serine/threonine kinase receptor interacting protein 1 (RIP/RIP1/RIPK1) was reported to have an important

role in programmed necrosis [10–12]. RIPK1 is also a crucial adaptor that mediates activation of the pro-survival transcription factor NF-kB by TNF, TLR3, and TLR4 [13–16]. The kinase function of RIPK1 is essential for programmed necrosis but dispensable for NF-kB activation [10–12], suggesting that programmed necrosis might be regulated at the level of activation of RIP1 kinase activity. It was reported that both necroptosis and cell death can be blocked by inhibiting RIPK1 [17–19]. Furthermore, RIPK1 was identified as a specific protein target for various paradigms of pathologic cell death, for which its inhibition has been demonstrated both in vitro and in vivo [17, 20–23]. Therefore, inhibition of RIPK1 was found to reduce the cell death through necroptosis and in addition, increase the chances of cell survival [16]. It was also postulated that RIPK1 resides at the crossroads of cell death and survival and thus, inhibition of its kinase activity tends it to move towards cell survival by activating NF-kB [24].

So far, necrostatin-1 and its analogues are the only known RIPK1 inhibitors [18]. Three RIPK1 protein structures with bound necrostatin analogues are available in Protein Data Bank (PDB) (PDB IDs 4ITH, 4ITI and 4ITJ). As yet, computational methods have not been used to identify inhibitors for RIPK1 and also, the conformational flexibility of the RIPK1 binding site has not been fully explored. Therefore, there is a need to discover novel RIPK1 inhibitors with structural diversity and varied scaffolds.

In computational drug design, pharmacophore modeling and pharmacophore based screening has been widely used in the virtual screening (VS), lead discovery and optimization [25–28]. Though pharmacophore based virtual screening of compounds is mostly stable, pharmacophore modeling is undergoing rapid advancement through the development and implementation of various strategies with respect to various contexts. The methodology of pharmacophore modeling is broadly classified into ligand-based and structure-based, depending on the availability of ligands and receptor proteins [29–31]. When a set of ligands that have been experimentally observed to interact with a specific protein target are available, ligand-based pharmacophore (LBP) modeling is done. When very few or no ligands are available for a protein target, then structure-based or receptor-based pharmacophore (SBP) modeling is done using an apo (protein only) or a holo (protein–ligand complex) protein structure.

In LBP generation, the selection of training set compounds play a key role. Different conformation generation algorithms produce different pharmacophore models [32–34]. Similarly, the selection of training set compounds has a great impact on the model generation. The use of same conformation generation algorithm with different training sets could generate completely different pharmacophore models of ligands interacting with the same protein target [35–37]. Since the quality of the pharmacophore model generated by ligand-based method can be considerably affected by various factors like the conformation generation method and the selection of training set molecules [38–40], SBP modeling has been depicted to be advantageous over ligand-based method. SBP generation is an ideal choice in the case of proteins like RIPK1 where no information other than only a few holo proteins is available. However, SBP model generation has its own limitations, depending on the available receptor conformations (apo) or the receptor-ligand complex (holo) protein structures.

Traditional SBP approaches use pharmacophore, derived from either a single apo [27] or holo protein [41] or from a multiple holo proteins [42]. Deriving SBP from a single holo protein structure would not be ideal because the derived pharmacophore will have the pharmacophoric features of that ligand only and the screened compounds may have same scaffold. This issue was addressed by generating a multicomplex-based pharmacophore model [43], from many holo protein structures, which determines all the key protein–ligand interactions. When a single apo protein is used, the derived pharmacophore will have the binding site features of that particular backbone and side chain conformations. This may not cover the entire pharmacophoric features of the protein binding site. Therefore, a combined strategy that involves building of pharmacophores covering all the features available in the binding site of the protein is required to screen compounds with varying scaffolds. In this context, we have developed an ensemble pharmacophore model by combining the pharmacophores derived from a combination of both the apo and holo proteins.

Conventional structure-based drug design (SBDD) methods use pharmacophore generation, pharmacophore screening and molecular docking methodologies in the discovery of small molecule inhibitors. Molecular docking is a commonly used VS method, which generates optimal binding modes of ligands in a given binding pocket and ranks these poses on the basis of docking scores. However, the accuracy of scoring functions remains a major challenge for the success of docking-based VS [44]. The docking output relatively depends on the binding of ligand to a given protein conformation. Sometimes, accurate scoring functions may give false results. For example, the ligand of 4ITI was self-docked with its receptor and also cross docked with 4ITJ (Fig. 1). Though both are reported to be RIPK1 proteins, the ligand binds to 4ITI with different conformation and comparatively less binding energy than with its native protein conformation, 4ITJ. This shows that the output of molecular docking not only necessarily depends on the scoring function but also on the

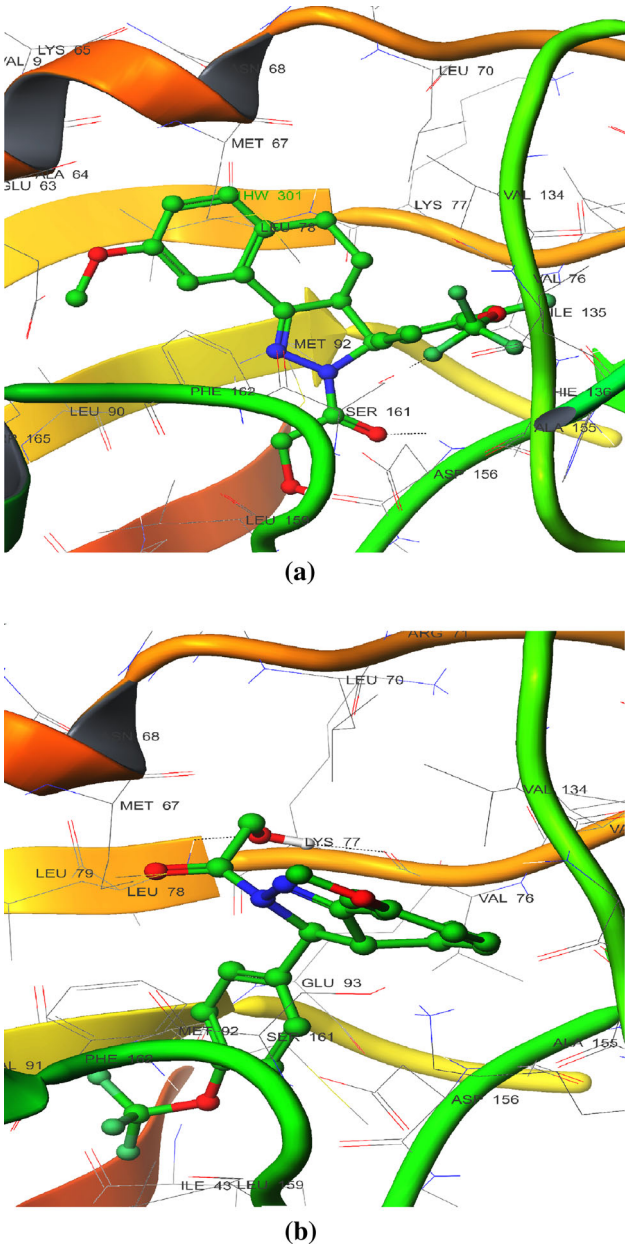

Fig. 1 **a** Ligand of 4ITI self-docked with its receptor, **b** ligand of 4ITI cross-docked with the receptor of 4ITJ

pharmacophore used for screening and the protein conformation used for docking. Though pharmacophores were derived from multiple holo or apo protein structures in previous approaches, the screened compounds were docked with only one of the protein structures [45, 46]. This would restrict/reduce the power of extracted pharmacophore.

So, a more robust SBDD approach is required in which all the protein conformations are involved in docking. In this study, we have developed a novel strategy known as Dual Ensemble Screening (DES) that involves ensemble pharmacophore based screening as well as ensemble docking based virtual screening. The workflow of DES is shown in Fig. 2.

Materials and methods

Protein structure preparation

The RIPK1 holo proteins (PDB Ids 4ITH, 4ITI and 4ITJ) were retrieved from PDB and were prepared using the protein preparation wizard of Schrodinger (Schrödinger LLC., Portland, USA). The chain A in all the structures were treated to add missing hydrogens, assign proper bond orders and delete water molecules beyond the 5 Å from the heterogeneous groups. The H-bonds were optimized using sample orientations. Finally, the protein structures were minimized to the default root mean square deviation (RMSD) value of 0.30 Å. The minimized protein structures were further considered for the pharmacophore analysis and docking.

Receptor grid generation and docking

Glide energy grids were generated for each of the prepared holo proteins. The co-crystallized ligand was differentiated from the active site of receptor. The grid was defined by a rectangular box surrounding the co-crystallized ligand. The atoms were scaled by van der Waals radii of 1.0 Å with the partial atomic charge less than 0.25 defaults. No constraints were defined. These grids were employed in all the docking studies.

Glide module has been used for all the docking protocol [47]. Ligand docking was performed using OPLS 2005 force field. The default settings as available in the software package were used for the refinement and docking calculations. The van der Waals radii were scaled using a default scaling factor of 0.80 and default partial cutoff charge of 0.15 to decrease the penalties. The option to output Glide XP descriptor information was chosen (Glide v5.7, Schrodinger, LLC, New York, NY), which deduces energy terms such as H-bond interactions, electrostatic interaction, hydrophobic enclosure, and π–π stacking interactions. The option to write per-residue interaction scores for residues within 12 Å of receptor grid center was also chosen. Finally, post docking minimization was implemented to optimize the ligand geometries.

E-pharmacophore mapping

Structure-based pharmacophores for the RIPK1 were extracted using the energy-optimized pharmacophore (e-pharmacophore) script of Schrodinger [48]. It is based on mapping of the energetic terms from the Glide XP score

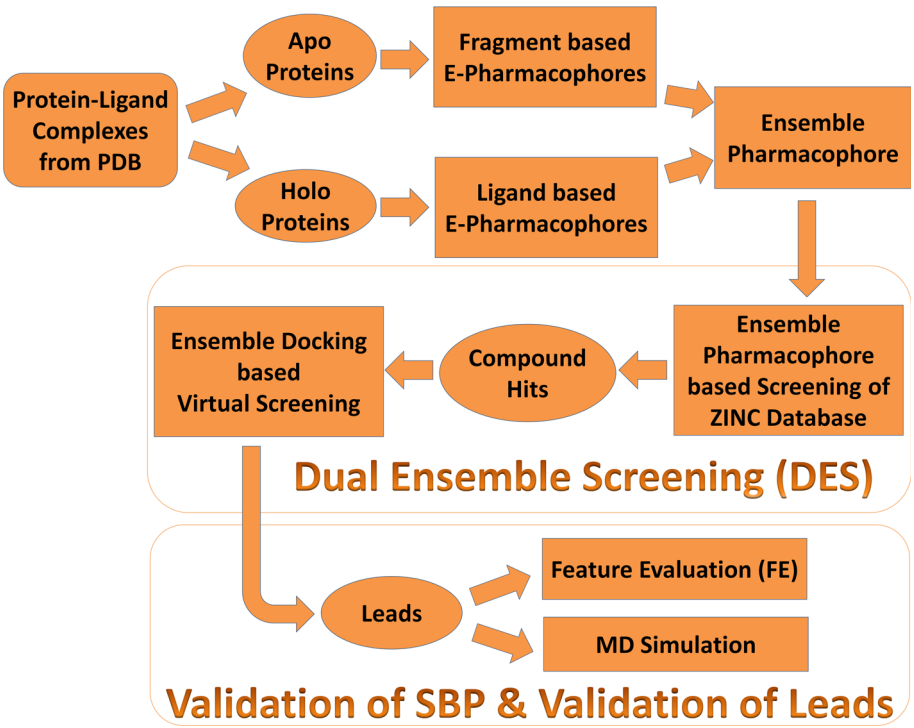

Fig. 2 Workflow of dual ensemble screening (DES) approach, developed and implemented in this study. It also involves validation of structure based pharmacophore (SBP) through feature evaluation and validation of leads through MD simulation studies

function onto atom centers. Both ligand-based and fragment-based e-pharmacophores were extracted. During ligand-based method, the three RIPK1 protein structures were treated as holo proteins and during fragment-based method, they were treated as apo proteins.

Pharmacophore features from holo proteins were extracted through ligand-based e-pharmacophore approach. Ligands were separated from their respective receptors and then re-docked using the Score in Place option in Glide XP.

Extraction of pharmacophoric features from apo proteins was attained through fragment-based e-pharmacophores. In order to extract these pharmacophores, glide fragment library was docked to each of the proteins using Glide XP. Glide fragment library consists of a set of 441 unique small fragments (1–7 ionization/tautomer variants; 6–37 atoms; MW range 32–226), derived from molecules in the medicinal chemistry literature.

The resultant pose viewer files in both the cases were used to generate pharmacophores through the e-pharmacophore script in Schrodinger software. This script extracts the energetic descriptors of the Glide XP score and assigns them to pharmacophore features. Pharmacophore sites were automatically generated from the protein–ligand complex with Phase, which provides a standard set of six pharmacophore features, H-bond acceptor (A), H-bond donor (D), hydrophobic group (H), negatively ionisable (N), positively ionisable region (P), and aromatic ring (R). The Glide XP scoring terms were computed, and the energies were mapped onto atoms. The pharmacophore sites were generated, and the Glide XP energies from the atoms that comprised each pharmacophore sites were summed up. These sites were then ranked based on the individual energies, and the most favourable sites were selected for the pharmacophore hypothesis.

Ensemble pharmacophore

The ligand-based and the fragment-based e-pharmacophores obtained from the RIPK1 proteins were carefully analysed for their diverse features. In order to incorporate all these features in the final pharmacophore, all the e-pharmacophores were superposed and their co-ordinates were taken and manually combined into a single file to generate an ensemble pharmacophore. If common features, corresponding to the same aminoacid feature in the binding site are present, then they were considered as a single feature and only one of them was represented in the ensemble pharmacophore. Further, if any positively ionisable regions (P) and negatively ionisable regions (N) are present, they were considered as donors and acceptors, respectively. Thus, this ensemble pharmacophore contains almost all the pharmacophoric features present in the binding site of the RIPK1 protein structures.

Ensemble pharmacophore-based screening

The ensemble pharmacophore was employed to screen the lead-like compounds ($\sim$2 million unique structure records)

in ZINC database [49] using Phase module. Explicit matching was the most important criteria for the e-pharmacophore approach. For filtering the database molecules, the distance matching tolerance was set to 2.0 Å as a balance between stringent and loose-fitting alignment. Further, the matching of a minimum of 4 sites was set as criteria. In the order of their fitness score, database hits were ranked to measure how well the aligned ligand conformer matched the hypothesis based on RMSD, site matching, vector alignments and volume terms. The compound hits thus obtained were considered for ensemble docking.

Ensemble docking

Due to the high dimensionality of the conformational space in protein binding site, involvement of target flexibility in docking studies still constitutes a difficult challenge. This especially applies to the high-throughput scenario, where the screening of hundreds of thousands compounds takes place. The use of multiple receptor conformations, in a sequential fashion, to perform docking is known as ensemble docking. This is a simple and powerful approach to incorporate binding site structural diversity in the docking process [50, 51].

The database hits obtained through ensemble pharmacophore-based screening were subjected to ligand preparation by the LigPrep module of the Schrodinger suite (LigPrepv2.3, Schrodinger, LLC, New York, NY). The ligands were processed to assign the suitable protonation states at physiological pH 7.2 ± 0.2. Conformer generation was carried out with the ConfGen torsional sampling by using OPLS 2005 force field.

Ensemble docking was performed using Glide in the Virtual Screening Wizard of Schrodinger suite. All the docking calculations were performed as mentioned in the earlier section. During ensemble docking, all the three grids corresponding to the three RIPK1 protein structures were selected and the prepared ligands were docked to each of these structures. The three docking results thus obtained were comparatively merged and the final output files that contain compounds in the order of their docking and Glide scores were obtained. Protein–ligand interactions such as H-bonds and hydrophobic interactions were visualized using LigPlot^{+} v.1.4 [52].

Molecular dynamics simulation

Based on the ensemble docking results, the top three ranked protein–ligand complexes with respect to the glide score (RIPK1—Lead 1, RIPK1—Lead 2 and RIPK1—Lead 3) were selected to carry out the Molecular Dynamics (MD) simulations using the Gromacs v4.5.5 software with Gromos53a6 force field [53–55]. PRODRG, a force field generation tool was used to generate topologies and parameters for ligands [56].

Prior to the execution of MD simulation, the system underwent 20,000 steps of steepest descent minimization in vacuum, followed by explicit solvation in a cubical water system (Petrova et al., 1985). Simple point charge water molecules (SPC/E) were used for solvation and the protein–ligand complex was placed in the center of a 87 Å × 87 Å × 87 Å cubic box. During the preparation procedure for the MD simulation, the ionizable residues of the protein were protonated without artifacts and the neutralization of the system was achieved by the addition of 69 Na^{+} and 61 Cl^{-} counter ions and a salt concentration of 0.1 M NaCl. The linear constraint (LINCS) algorithm was applied to fix all hydrogen related bond lengths, facilitating the use of a 2-fs time step. Particle Mesh Ewald (PME) was employed to treat long-range electrostatic interactions [57]. A cut-off of 1.0 nm was used for both van der Waals and the PME direct-space component of electrostatic interactions. The SHAKE algorithm was employed to constrain all bond lengths involving H-atoms.

Further, 20,000 steps of steepest descent energy minimization were employed on the solvated system to properly allow the solvent molecules to adjust/relax around the protein. After energy minimization, all the systems were equilibrated for 100 ps with NVT and NPT ensemble equilibration protocol for about 50,000 steps, with the protein backbone atoms restrained in order to prevent adsorption before equilibration. Extensive MD simulations were then performed for a total of 20 ns under a constant number of particles at constant temperature of 310 K using Berendsen's method [58] and at a constant pressure of 1 bar with a 2.0 fs time step. Pressure and temperature coupling constants were 0.4 ps. Analyses were carried out using the Gromacs and visual molecular dynamics (VMD) analysis package [59].

Results and discussion

Ligand based e-pharmacophores

Ligand based e-pharmacophores were derived from the three RIPK1 protein–ligand complexes. The e-pharmacophore derived from 4ITH consists of five pharmacophore features (1A, 2D and 2R), with hydrogen bond acceptor and donors corresponding to Val 76, Asp 156 and Ser 161 amino acids (Fig. 3a). The e-pharmacophore derived from 4ITI consists of six pharmacophore features (2A, 1D, 1H and 2R), with hydrogen bond acceptors and donor corresponding to Asp 156 and Ser 161 amino acids (Fig. 3b). Similarly, the e-pharmacophore derived from 4ITJ consists

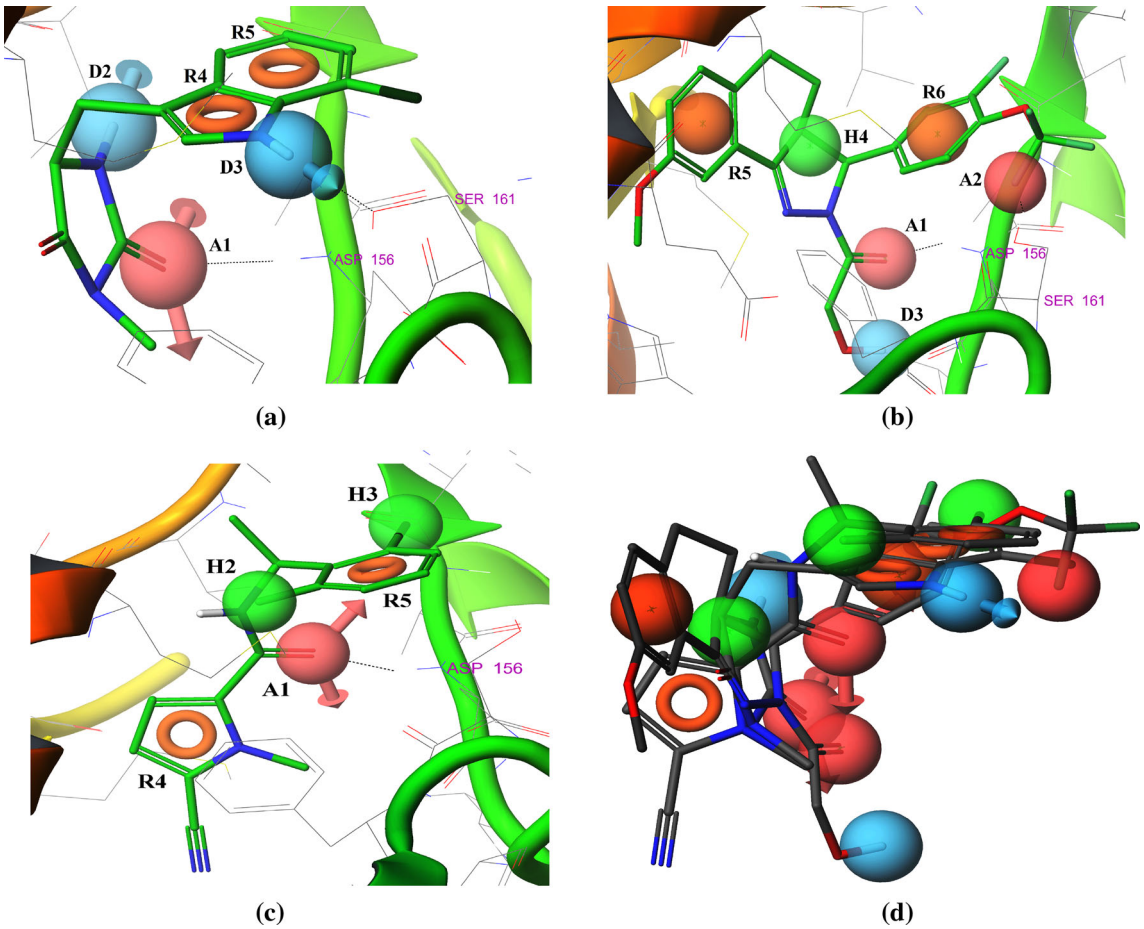

Fig. 3 Ligand based e-pharmacophores derived from the holo proteins of **a** 4ITH, **b** 4ITI, **c** 4ITJ and **d** alignment of the three ligands and their e-pharmacophores

of five pharmacophore features (1A, 2H and 2R), with hydrogen bond acceptor corresponding to Asp 156 amino acid (Fig. 3c). If we compare the features in these e-pharmacophores, then only one acceptor and one aromatic ring feature are common in all the three molecules (Fig. 3d). A1 in Fig. 3a, b, c are similar. Further, R4 in Fig. 3a, R6 in Fig. 3b and R5 in Fig. 3c are similar. The features D2, D3 and R5 in Fig. 3a, A2, D3, H4 and R5 in Fig. 3b and H2, H3 and R4 in Fig. 3c are specific to the respective ligand molecules. Therefore, the pharmacophore features in ligand based pharmacophores are mapped to Val 76, Asp 156 and Ser 161 amino acids.

Fragment based e-pharmacophores

RIPK1 protein structures without their ligands were treated as apo proteins and the pharmacophoric features of the entire binding site of these proteins were extracted through fragment based e-pharmacophore approach. Three fragment based e-pharmacophores were derived from their respective protein structures.

The e-pharmacophore derived from 4ITH consists of eight pharmacophore features (2A, 2D, 1P, 1H and 2R) (Fig. 4a), with hydrogen bond acceptors and donors corresponding to Met 67, Leu 70, Val 76,Leu 78 and Asp 156 amino acids. The e-pharmacophore derived from 4ITI consists of nine pharmacophore features (3A, 3D, 1H and 2R) (Fig. 4b), with hydrogen bond acceptors and donors corresponding to Leu 70, Val 76,Leu 78,Asp 156 and Ser 161 amino acids. Similarly, the e-pharmacophore derived from 4ITJ consists of ten pharmacophore features (3A, 3D, 1P, 1H and 2R) (Fig. 4c), with hydrogen bond acceptors and donors corresponding to Met 67, Leu 70, Val 76, Ile 154, Asp 156 and Ser 161 amino acids. The pharmacophore features in fragment based e-pharmacophores are mapped to Met 67, Leu 70, Val 76,Leu 78, Ile 154, Asp 156 and Ser 161 amino acids. If we compare the features in the fragment based e-pharmacophores, then A1 in Fig. 4a is similar to A1 in Fig. 4b, c. The feature A2 in Fig. 4a is similar to A3 in Fig. 4b, c. The feature A2 in Fig. 4b is similar to A2 in Fig. 4c. The feature D3 in Fig. 4a is similar to D4 in Fig. 4b. The feature D4 in Fig. 4a is

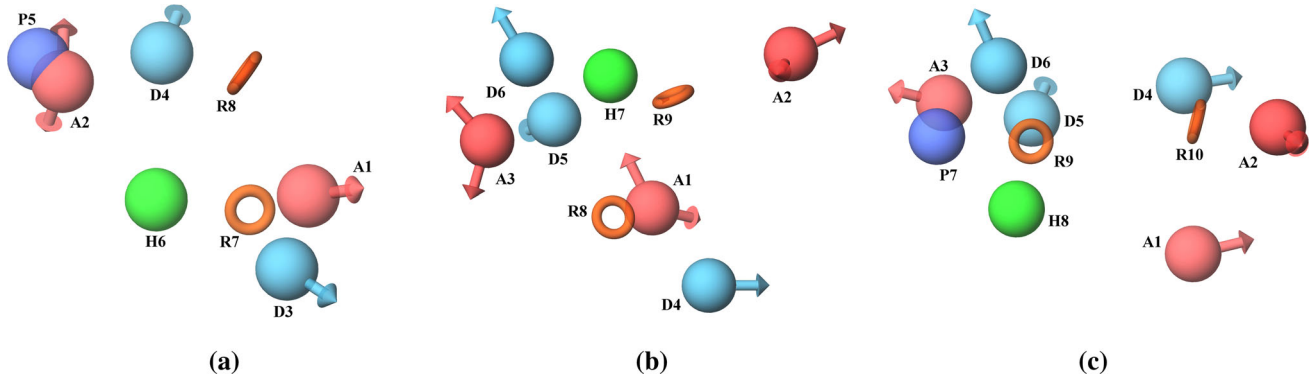

Fig. 4 Fragment based e-pharmacophores derived from the apo proteins of **a** 4ITH, **b** 4ITI and **c** 4ITJ

similar to D6 in Fig. 4b, c. The feature D5 in Fig. 4b is similar to D5 in Fig. 4c. The feature R7 in Fig. 4a is similar to R8 in Fig. 4b. The feature R8 in Fig. 4a is similar to R9 in Fig. 4b and R10 in Fig. 4c.

If we compare the features in the fragment based e-pharmacophores to their corresponding ligand based e-pharmacophores, then A1, D2 and R4 in Fig. 3a is similar to A1, D4 and R8 in Fig. 4a respectively. The features A1, A2, D3 and R6 in Fig. 3b are similar to A1, A2, D4 and R9 in Fig. 4b respectively. The features A1 and R5 in Fig. 3c are similar to A1 and R10 in Fig. 4c respectively. Thus, when compared to ligand based e-pharmacophores, the fragment based e-pharmacophores have covered extra features corresponding to Met 67, Leu 70, Leu 78 and Ile 154 amino acids. Almost all the features identified through ligand based e-pharmacophores were also identified through fragment based e-pharmacophores. However, in some cases, the fragment based e-pharmacophore extraction might not have identified certain features that were identified through the ligand based approach. This may be due to the reasons such as the features may be ligand specific and/or also may be due to the constraints in the availability of the fragments. Due to these reasons, a combination of both the ligand based and fragment based e-pharmacophore extraction methods was considered in this study, in order to identify all the possible features present in the binding site.

Ensemble pharmacophore

By combining all the ligand-based and fragment-based e-pharmacophore features, an integrated pharmacophore known as ensemble pharmacophore was created, which includes the features corresponding to all the key amino acids in the RIPK1 binding site. However, the hydrophobic features that were extracted had very less score. Hence, in order to minimize the features in the ensemble pharmacophore and in turn avoid the number of false positives

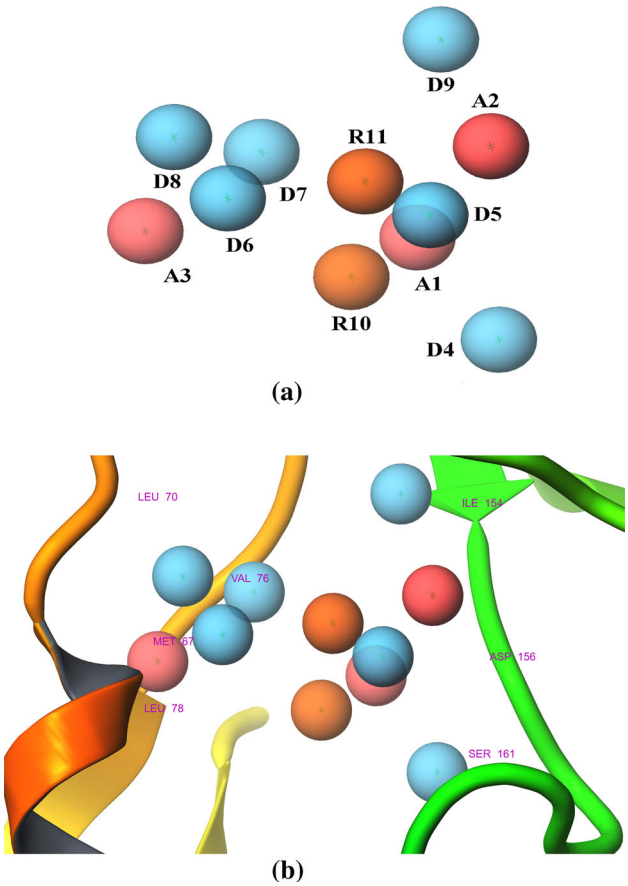

Fig. 5 **a** Ensemble pharmacophore derived by combing the ligand based and fragment based e-pharmacophores, **b** ensemble pharmacophore mapped on to the binding site of RIPK1

identified during the screening process, only the H-bond acceptors, H-bond donors and aromatic features were considered during the construction of ensemble pharmacophore. Thus, the ensemble pharmacophore consists of eleven pharmacophore features namely 3A, 6D and 2R (Fig. 5a) corresponding to Met 67, Leu 70, Val 76, Leu 78, Ile 154, Asp 156 and Ser 161 amino acids (Fig. 5b). If we

Table 1 Ensemble pharmacophore features, their respective co-ordinates and corresponding amino acids in the binding site of RIPK1 protein

Sl no.	Feature type	Feature label	X	Y	Z	Corresponding aminoacid
1	A	A1	7.824740	15.983200	33.824800	Leu 78
2	A	A2	7.265640	13.183500	28.839200	Asp 156
3	A	A3	3.672600	8.050270	31.424700	Ser 161
4	D	D4	5.046720	13.715600	26.844800	Asp 156
5	D	D5	8.163100	13.501600	34.772400	Leu 70
6	D	D6	9.126590	13.592500	32.194600	Val 76
7	D	D7	6.011190	13.292500	34.013400	Met 67
8	D	D8	9.498540	9.196160	30.563600	Ile 154
9	D	D9	3.986080	10.581000	31.127900	Ser 161
10	R	R10	6.656320	14.479300	29.785700	Many
11	R	R11	5.491500	11.227000	32.018400	Many

compare this ensemble pharmacophore features with the ligand-based and fragment-based e-pharmacophore features, then A1 is similar to A1 in Fig. 4a, b, c. The feature A2 is similar to A2 in Fig. 4b, c. The feature A3 is similar to A2 in Fig. 4a and A3 in Fig. 4b, c. The feature D4 is similar to D3 in Fig. 4a and D4 in Fig. 4b. The feature D5 is similar to D3 in Fig. 3a. The feature D6 is similar to D5 in Fig. 4b, c. The feature D7 is similar to D4 in Fig. 4a and D6 in Fig. 4b and Fig. 4c. The feature D8 is similar to P5 in Fig. 4a and P7 in Fig. 4c. The feature D9 is similar to D4 in Fig. 4c. The feature R10 is similar to R7 in Fig. 4a and R8 in Fig. 4b. The feature R11 is similar to R8 in Fig. 4a, R9 in Fig. 4b and R10 in Fig. 4c. The numbering of the features differs in all the e-pharmacophores since the number of features differ in these pharmacophores. Thus, this ensemble pharmacophore span the entire binding site of RIPK1 protein (Table 1), covering all the important amino acids that may probably involve in the interactions with the ligands.

Dual ensemble screening

In this study, we have developed and implemented the DES strategy that involves screening of compounds using two ensembles namely, ensemble pharmacophore and ensemble docking. Initially, ensemble pharmacophore was employed for pharmacophore based screening of ZINC database. A total of 789,351 compound hits were retrieved from the ZINC database. Later, these hits were subjected to docking based virtual screening through ensemble docking, which involves subsequent docking of compound hits to all the three RIPK1 protein structures.

The lead compounds obtained through DES had diverse structures with varying scaffolds. They covered all the features present in the ensemble pharmacophore. The top three lead compounds are shown in Fig. 6. These leads matched most of the pharmacophore features. They exhibited good interactions with the desired amino acids in the binding site (Fig. 7). Further, they showed good fitness scores and glide scores (Table 2). Lead 1 showed hydrogen bonding with Leu 70, Val 76, Asp 156 and Ser 161 amino acids (Fig. 7a). In this case, Val 76, Asp 156 and Ser 161 are the amino acids corresponding to the features obtained through ligand based pharmacophores, whereas Leu 70 is the amino acid corresponding to the feature obtained through fragment based pharmacophore. This is an exemplary case to show that a combination of ligand based and fragment based pharmacophores is required to explore the entire binding site and to identify potent inhibitors. Further, Lead 2 formed hydrogen bonding with Leu 70 (Fig. 7b), demonstrating that the pharmacophore features extracted from apo proteins are equally efficient compared to holo proteins. This underlines the use of apo proteins or a combination of apo and holo proteins rather than the conventional use of holo proteins alone, for structure based pharmacophore extraction, as seen in most of the virtual screening strategies.

Validation of dual ensemble screening

In order to check the reliability of our methodology involving ensemble pharmacophore and ensemble docking, validation of dual ensemble screening was carried out using known RIPK1 inhibitors. There are almost ten RIPK1 inhibitors reported in the literature [60–64]. The structures of these compounds were drawn using ChemSketch and the 3D structures were generated through the structure file generator server hosted by NCI. The preparation of these ligands and the generation of conformers were carried out as described in the earlier sections. These inhibitors were then seeded randomly into the ZINC database compounds on which pharmacophore based screening was carried out. Further, the screened inhibitors were subjected to ensemble docking.

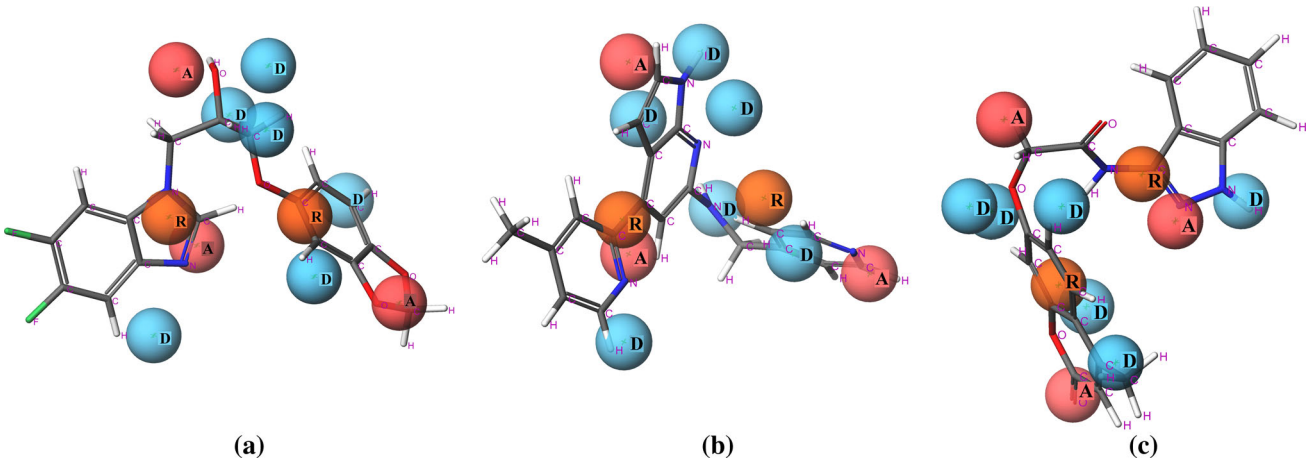

Fig. 6 Matching of ensemble pharmacophoric features with the top three lead compounds obtained through ensemble docking **a** Lead 1, **b** Lead 2, and **c** Lead 3

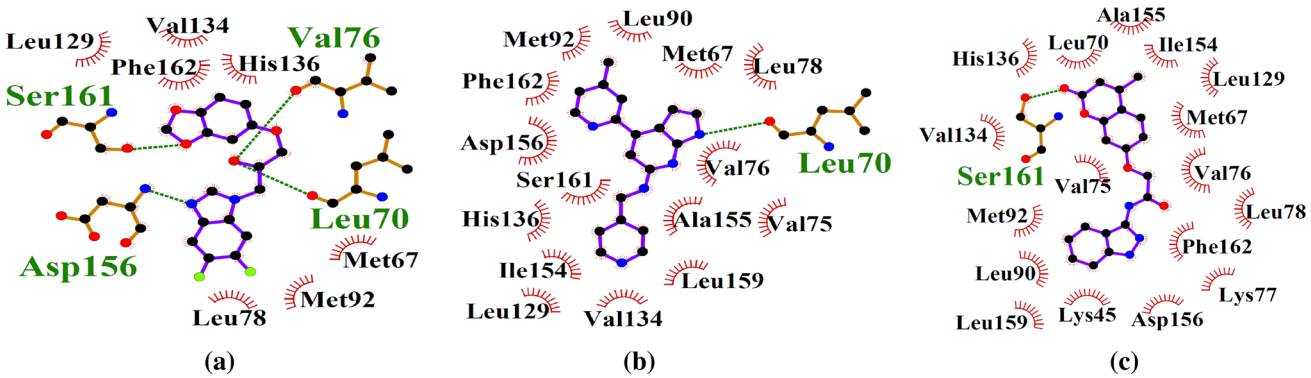

Fig. 7 LigPlot showing hydrogen bonds and hydrophobic interactions of **a** Lead 1, **b** Lead 2 and **c** Lead 3, with RIPK1 protein

Table 2 Glide docking output of the three lead molecules

Ligand	Zinc ID	Fitness	Glide score	Glide energy (kcal/mol)	H-bond interactions
Lead 1	ZINC71828321	1.282211	−12.827719	−55.550181	Leu 70, Val 76
Lead 2	ZINC72454060	1.144806	−12.749376	−48.952555	Leu 70
Lead 3	ZINC79476695	1.134246	−12.463987	−53.710299	Ser 161

During DES, the ensemble pharmacophore could retrieve all the known RIPK1 inhibitors. These inhibitors matched most of the pharmacophoric features (Fig. 8). Also, the ligands in the RIPK1 PDB structures, which were used to derive the ligand based e-pharmacophores, matched their corresponding features exactly in the ensemble pharmacophore (Fig. 8a, b). The ligand in Fig. 8a matched with the features A1, D5, D7, R10 and R11 of ensemble pharmacophore that corresponds to the features A1, D3, D2 and R4, respectively of the ligand based e-pharmacophore in Fig. 3a. Similarly, the ligand in Fig. 8b matched with the features A1, A2, D4, R11 and R10 of ensemble pharmacophore that corresponds to the features A1, A2, D3 and R6, respectively of the ligand based e-pharmacophore in Fig. 3b. Therefore, the ensemble pharmacophore represented all the experimentally observed interactions.

However, ensemble docking could retrieve only eight known inhibitors. The inhibitors namely cpd8 and cpd20 [64] could not be retrieved. This may be due to the reason that these inhibitors may bind to a different RIPK1 conformation and also to different amino acids that are not corresponding to the ensemble pharmacophore. When the docked inhibitors were considered, they showed interactions with only the amino acids corresponding to the ensemble pharmacophore (Fig. 8). Further, the inhibitors Nec-1 and Nec-3 showed similar interactions and binding modes with their analogues 7-Cl-O-Nec-1 (ligand in 4ITH) and Nec-3a (ligand in 4ITI), respectively (Figs. 8, 9).

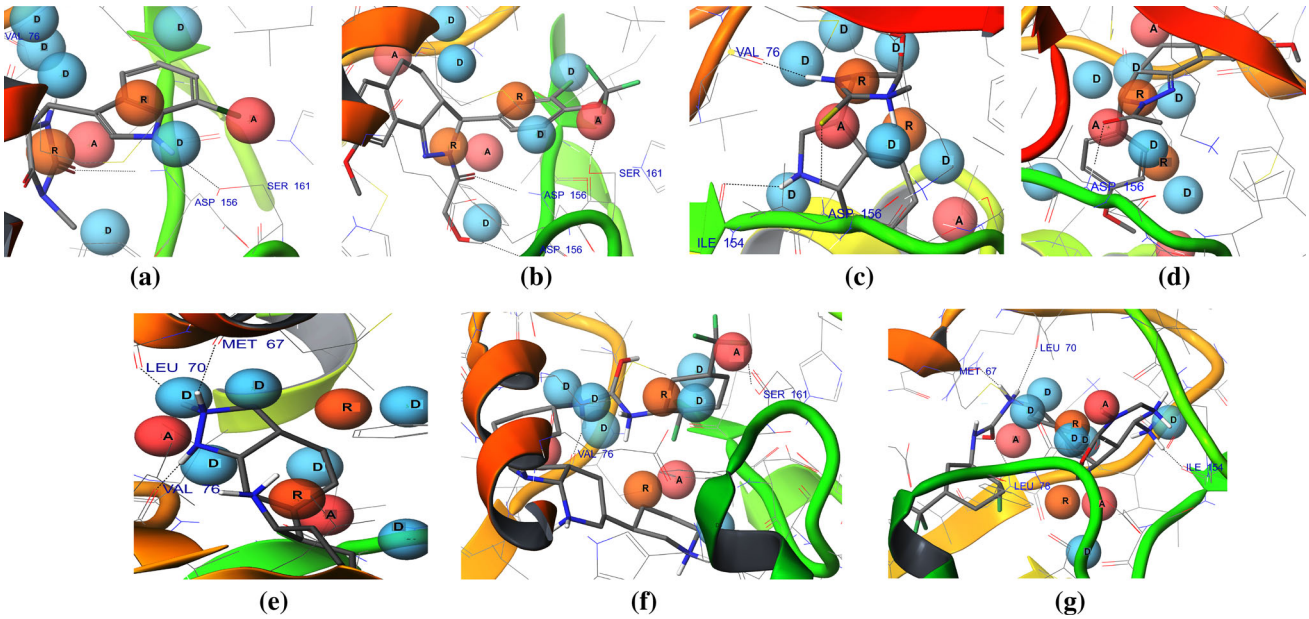

Fig. 8 Interactions of known RIPK1 inhibitors with the amino acids corresponding to the ensemble pharmacophore in the binding site. **a** 7-Cl-O-Nec-1 (ligand in 4ITH), **b** Nec-3a (ligand in 4ITI), **c** Nec-1, **d** Nec-3, **e** Nec-21, **f** cpd 18 and **g** cpd 27

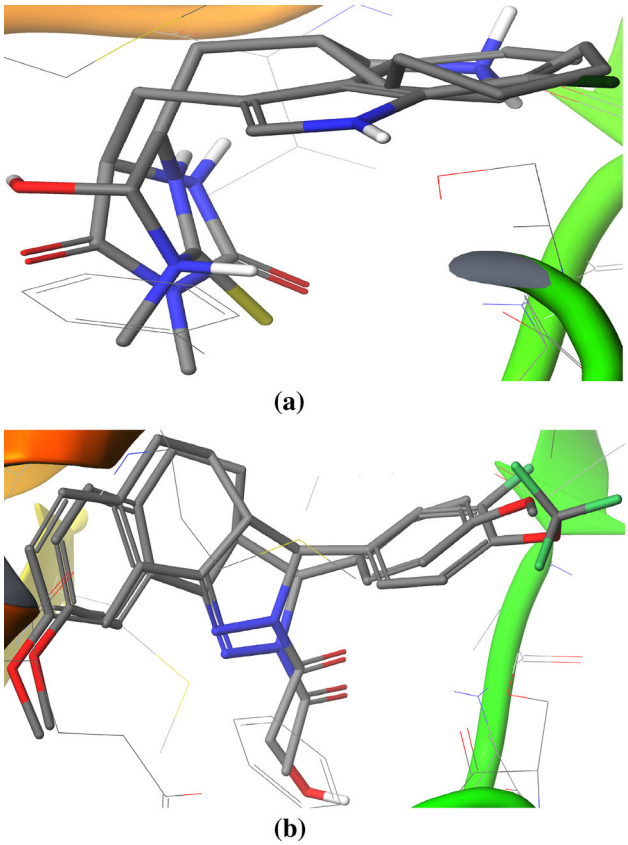

Fig. 9 Alignment of the docked conformations of the known RIPK1 inhibitors with the ligands in the RIPK1 PDB structures. **a** Nec-1 aligned with 7-Cl-O-Nec-1 (ligand in 4ITH) and **b** Nec-3 aligned with Nec-3a (ligand in 4ITI)

The most popularly used and the simplest metric method to evaluate the effectiveness of a virtual screening method is the enrichment at a given percentage of the database screened [65, 66]. The Enrichment Factor (EF) is defined as:

$$EF^{x\%} = \frac{n\,(\text{active at } x\%)/n\,(x\%)}{n\,(\text{all active})/n\,(\text{all})}$$

where n(active at x%) is the number of active ligands identified in the top x% of the database screened, n(x%) is the number of compounds screened at top x% of the database, n(all active) is the number of active ligands in entire database, and n(all) is the number of compounds in entire database [67].

Both the ensemble pharmacophore based screening and the ensemble docking based virtual screening methodologies were validated using the early enrichment factors at 1 and 5 % of the database screened. For ensemble pharmacophore based screening, the $EF^{1\%}$ and $EF^{5\%}$ were 30 and 8, respectively, and for ensemble docking based virtual screening, the $EF^{1\%}$ and $EF^{5\%}$ were 40 and 14, respectively. This shows that our dual ensemble screening method is considerably reliable.

Feature evaluation

In order to find whether the lead compounds contain the desired pharmacophore features and also to assess whether they interact with the amino acids corresponding to the features of ensemble pharmacophore, we have followed a

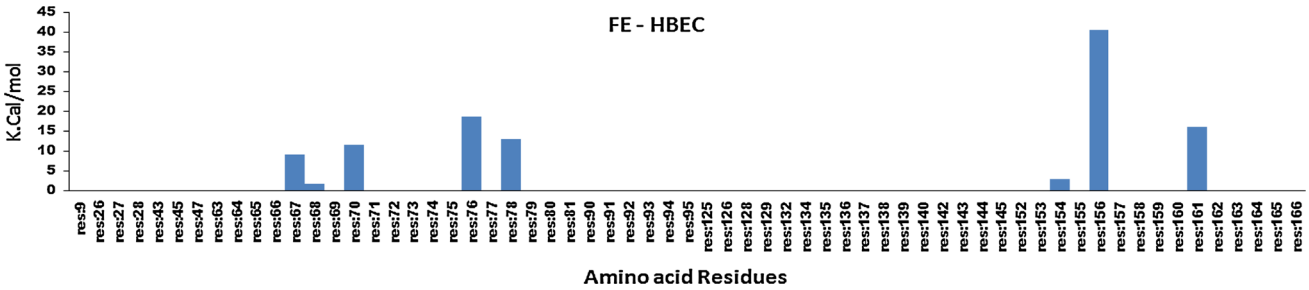

Fig. 10 *Graph* showing H-bond energy contribution (HBEC) of each amino acid residue present within 12 Å of receptor grid center

novel approach known as feature evaluation (FE). In this method, per-residue interaction scores of residues, which were obtained during Glide XP docking, were used to calculate H-bond energy contribution (HBEC) and total energy contribution (TEC) of amino acids within 12 Å of receptor grid center. HBEC of an amino acid is calculated by adding the H-bond energies of all the ligands with that amino acid. Similarly, TEC of an amino acid is calculated by adding the interaction energies of all the ligands with that amino acid. HBEC denotes the H-bond energy contributed by each residue towards the interaction energy with the ligands and from this, all the amino acid residues that are involved in hydrogen bonding could be known. TEC denotes the total interaction energy contributed by each amino acid residue with the ligands and by calculating this, the residues that contributed more to the interaction energy of the ligands could be identified.

$$\text{HBEC of aminoacid X} = \sum_{N=0}^{50}$$

(Hydrogen bonding energy of ligand N with aminoacid X)

$$\text{TEC of aminoacid X} = \sum_{N=0}^{50}$$

(Interaction energy of ligand N with aminoacid X)

HBEC of each amino acid were calculated for the top 50 lead molecules and plotted as a graph (Fig. 10). It was found that the residues 67, 68, 70, 76, 78, 154, 156 and 161 formed H-bonds with the leads. This shows that the leads contain the required pharmacophore features, which eventually made them to interact with the corresponding amino acids. Further, from the graph, it can be seen that, except for residue 68, only the seven amino acids corresponding to the pharmacophore features of ensemble pharmacophore were involved in H-bonding. This shows that during pharmacophore mapping, all the features present in the binding site were extracted in the form of ensemble pharmacophore and were reflected during ensemble docking.

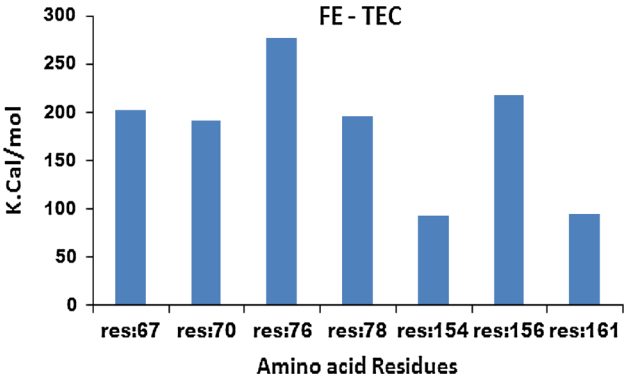

Fig. 11 *Graph* showing the total energy contribution (TEC) of each of the seven amino acids that exhibits HBEC and also corresponds to the ensemble pharmacophore features

In order to find whether the amino acids corresponding to the features extracted from apo proteins have reasonable role, the extent of contribution of each of the seven amino acids towards the interaction energy of the ligands was calculated through TEC and was plotted as a graph (Fig. 11). It can be noted that the residues 67, 70, 78 and 154 contribute to a considerable extent to the interaction energy of the ligands. This demonstrates that the extraction of these features was not due to some sort of coincidence, but rather due to a more focused approach. Therefore, FE approach would remarkably help to validate the structure based pharmacophores.

Validation of leads

The binding and interaction of top three leads with the RIPK1 protein was further validated through MD simulation studies. The alignment of protein–ligand complexes, obtained through docking and simulation, shows that the ligands bind to the protein with similar conformational modes (Fig. 12) and this confirms the interactions of the ligands obtained during docking studies. Further, it was observed that these leads remained in the binding site throughout the simulation. The potential energy and the RMSD of the protein backbone and ligand in the

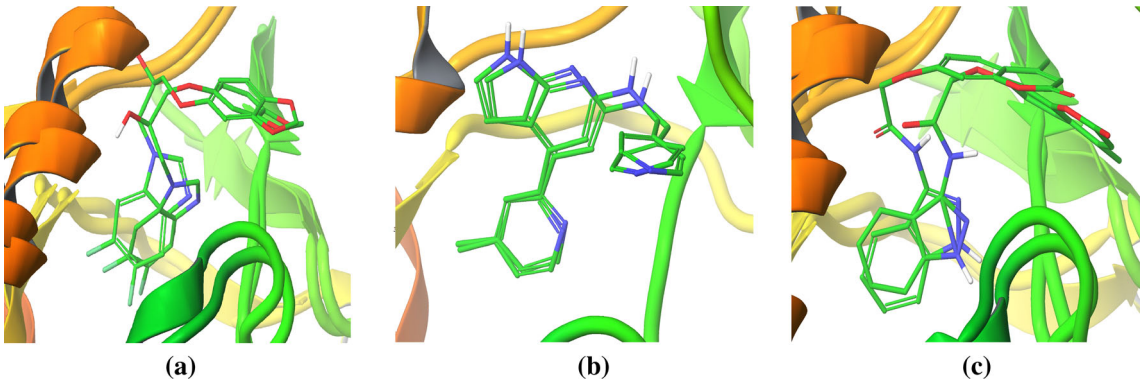

Fig. 12 Comparison of ligand binding conformations during docking and MD simulation studies through alignment of the resultant protein–ligand complexes containing **a** Lead 1, **b** Lead 2 and **c** Lead 3

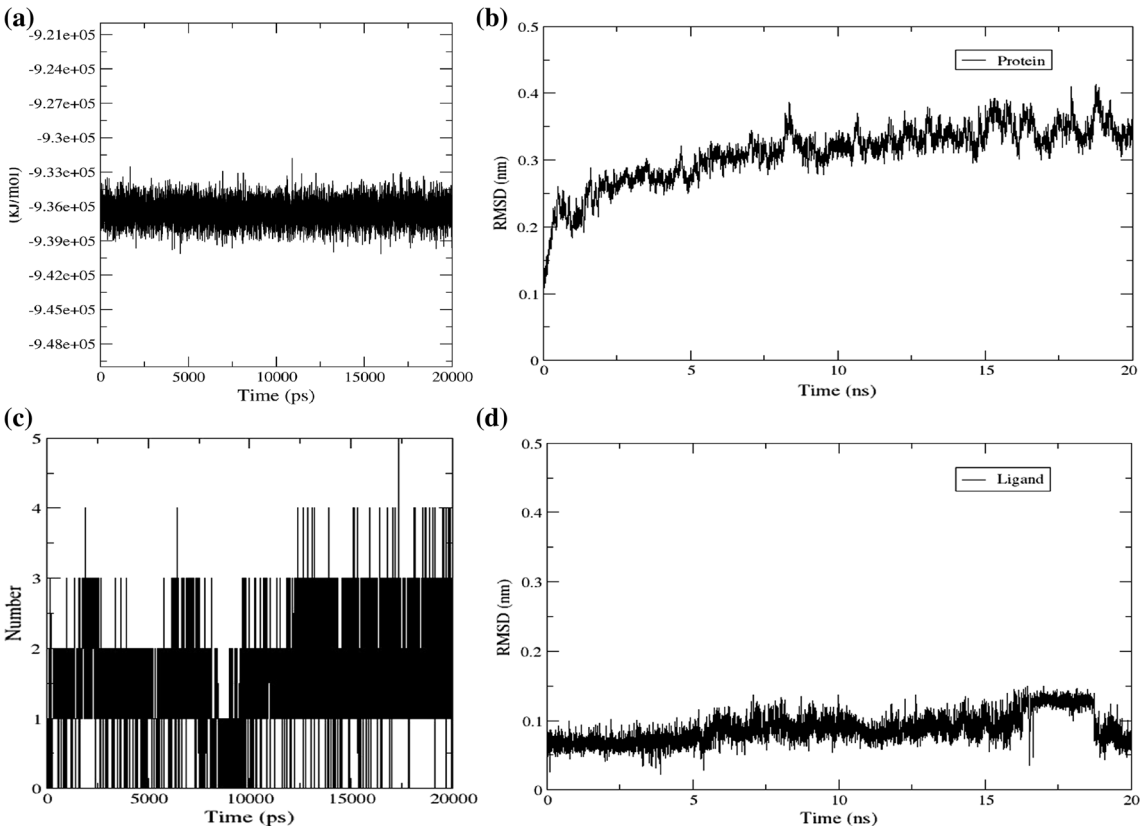

Fig. 13 MD simulation output of Lead 1 with RIPK1 protein. **a** Potential energy of the protein–ligand complex during simulation, **b** RMSD of the protein backbone, **c** hydrogen bonds and **d** RMSD of the ligand (Lead 1)

complexes were steady and they became stable during the course of simulation (Figs. 13, 14, 15).

Conclusions

Identification of diverse and potent small molecule inhibitors through SBDD becomes a daunting task when very few holo proteins are available, as in the case of RIPK1, since the pharmacophores derived from them does not serve the purpose. Therefore, a more integrated approach that takes all the pharmacophore features of the binding site into account is necessary. In this study, we have used a combination of fragment based e-pharmacophores and ligand based e-pharmacophores derived from apo and holo proteins respectively, to build an ensemble pharmacophore.

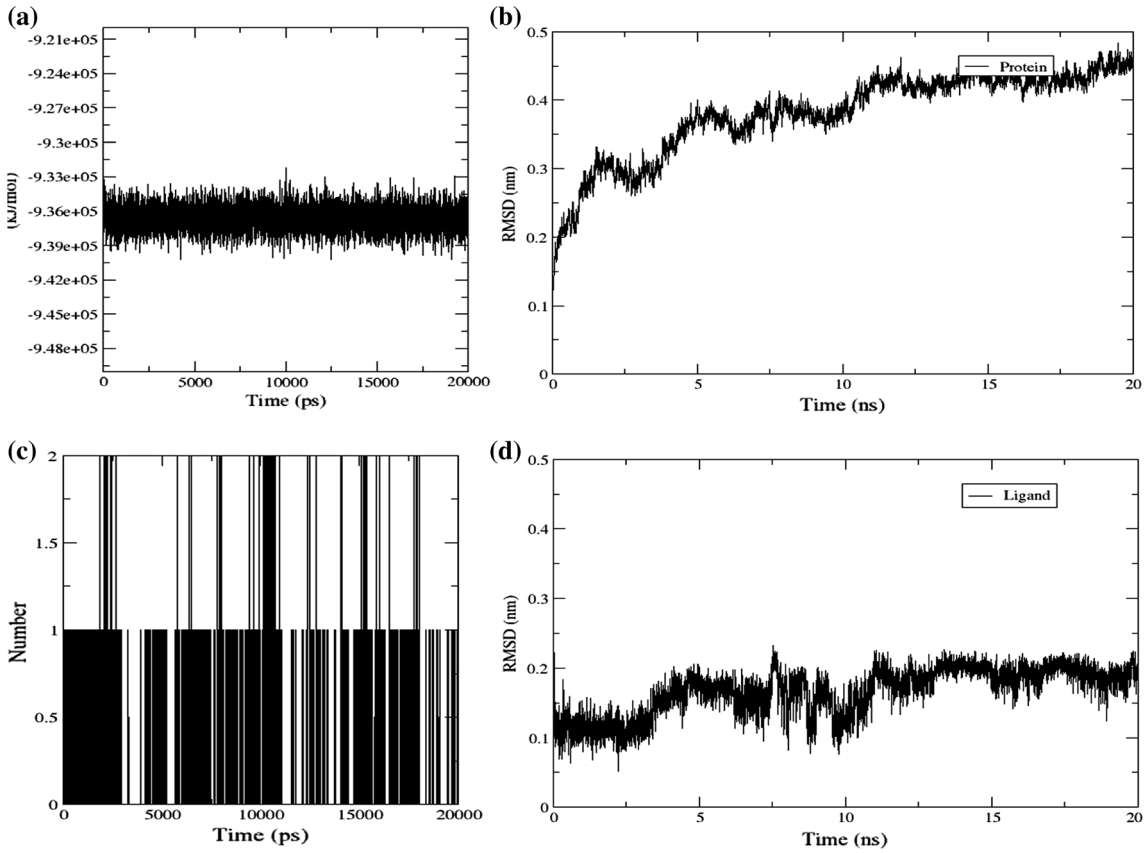

Fig. 14 MD simulation output of Lead 2 with RIPK1 protein. **a** Potential energy of the protein–ligand complex during simulation, **b** RMSD of the protein backbone, **c** hydrogen bonds and **d** RMSD of the ligand (Lead 2)

This ensemble pharmacophore incorporates the entire pharmacophoric features present in the binding site. The validation of features in the structure based pharmacophores is very challenging since methods rarely exist for this purpose. The feature evaluation approach, used in this study, has addressed this problem to a greater extent. Interaction of leads with the amino acids corresponding to the pharmacophore features only, proves that almost all the features present in the binding site of RIPK1 were successfully captured.

When multiple protein structures are used for pharmacophore development, there is a huge possibility to achieve false docking results, in spite of good scoring functions, if appropriate protein structures are not used during docking. The ensemble docking, employed in this study, helps to overcome this problem. Here, all the protein structures that were used for ensemble pharmacophore extraction were subsequently engaged in docking. This DES strategy involving ensemble pharmacophore and ensemble docking would facilitate improved SBDD. Further, this methodology was validated through the early enrichment factors using known RIPK1 inhibitors. These inhibitors exhibited interactions with the aminoacids corresponding to the ensemble pharmacophore. They also showed binding modes and interactions similar to their analogues present in the RIPK1 PDB structures. Identification of RIPK1 inhibitors has greater therapeutic relevance since inhibition of necroptosis pathway is desirable in many diseases. This newly developed computational strategy that involved the dual ensemble screening approach, feature evaluation and MD simulation studies altogether was implemented in the identification of novel small molecule inhibitors of RIPK1. Further optimization of these lead compounds could result in more potent therapeutic molecules against various diseases involving necroptosis.

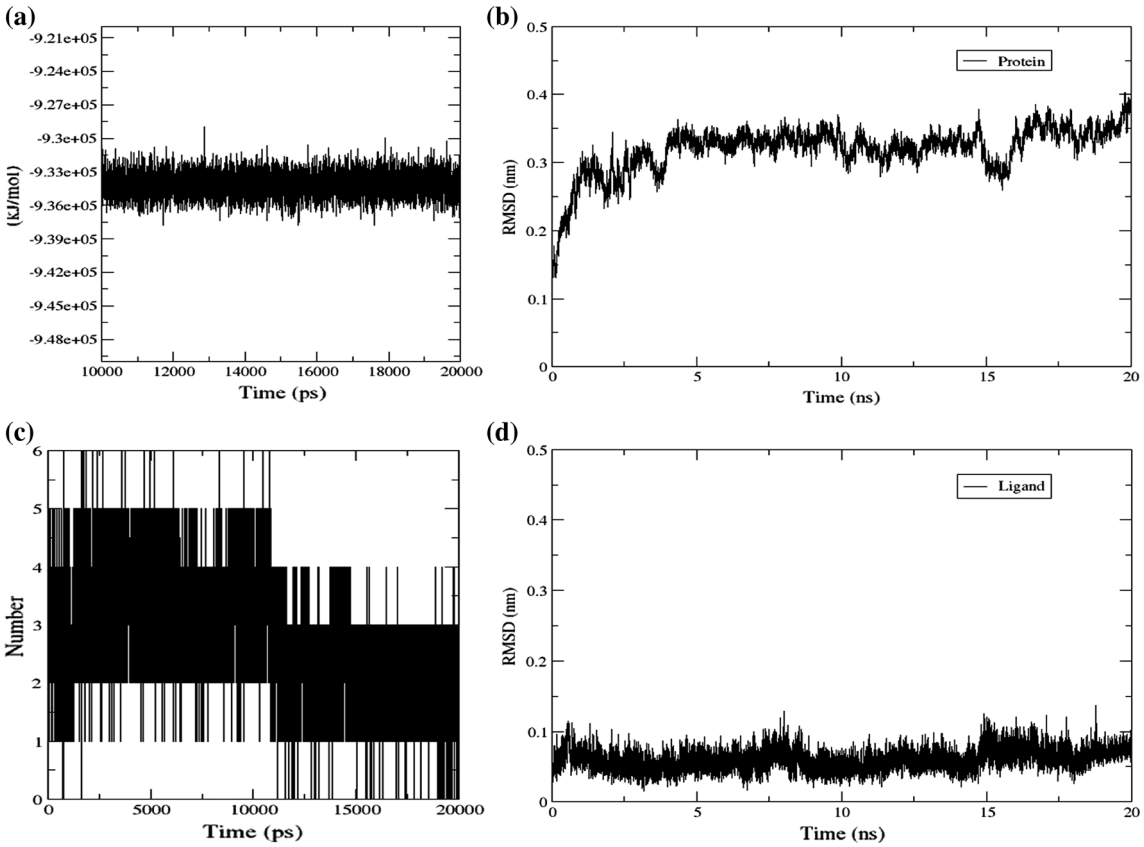

Fig. 15 MD simulation output of Lead 3 with RIPK1 protein. **a** Potential energy of the protein–ligand complex during simulation, **b** RMSD of the protein backbone, **c** hydrogen bonds and **d** RMSD of the ligand (Lead 3)

References

1. Bramlett HM, Dietrich WD (2004) Pathophysiology of cerebral ischemia and brain trauma: similarities and differences. J Cereb Blood Flow Metab 24:133–150. doi:10.1097/01.WCB.0000111614.19196.04
2. Tsujimoto Y, Shimizu S (2005) Another way to die: autophagic programmed cell death. Cell Death Differ S2:1528–1534. doi:10.1038/sj.cdd.4401777
3. Thornton C, Rousset CI, Kichev A, Miyakuni Y, Vontell R, Baburamani AA, Fleiss B, Gressens P, Hagberg H (2012) Molecular mechanisms of neonatal brain injury. Neurol Res Int 2012:506320. doi:10.1155/2012/506320
4. Zhang DW, Shao J, Lin J, Zhang N, Lu BJ, Lin SC, Dong MQ, Han J (2009) RIP3, an energy metabolism regulator that switches TNF-induced cell death from apoptosis to necrosis. Science 325:332–336. doi:10.1126/science.1172308
5. He S, Wang L, Miao L, Wang T, Du F, Zhao L, Wang X (2009) Receptor interacting protein kinase-3 determines cellular necrotic response to TNF-alpha. Cell 137:1100–1111. doi:10.1016/j.cell.2009.05.021
6. Pinheiro da Silva F, Nizet V (2009) Cell death during sepsis: integration of disintegration in the inflammatory response to overwhelming infection. Apoptosis 14:509–521. doi:10.1007/s10495-009-0320-3
7. Fayaz SM, Suvanish Kumar V, Rajanikant GK (2014) Necroptosis: who knew there were so many interesting ways to die? CNS Neurol Disord: Drug Targets 13:42–51. doi:10.2174/18715273113126660189
8. Linkermann A, Hackl MJ, Kunzendorf U, Walczak H, Krautwald S, Jevnikar AM (2013) Necroptosis in immunity and ischemia-reperfusion injury. Am J Transplant 13:2797–2804. doi:10.1111/ajt.12448
9. Mehta SL, Manhas N, Raghubir R (2007) Molecular targets in cerebral ischemia for developing novel therapeutics. Brain Res Rev 54:34–66. doi:10.1016/j.brainresrev.2006.11.003
10. Chan FK, Shisler J, Bixby JG, Felices M, Zheng L, Appel M, Orenstein J, Moss B, Lenardo MJ (2003) A role for tumor necrosis factor receptor-2 and receptor-interacting protein in programmed necrosis and antiviral responses. J Biol Chem 278:51613–51621. doi:10.1074/jbc.M305633200
11. Holler N, Zaru R, Micheau O, Thome M, Attinger A, Valitutti S, Bodmer JL, Schneider P, Seed B, Tschopp J (2000) Fas triggers an alternative, caspase-8-independent cell death pathway using the kinase RIP as effector molecule. Nat Immunol 1:489–495. doi:10.1038/82732
12. Lin Y, Choksi S, Shen HM, Yang QF, Hur GM, Kim YS, Tran JH, Nedospasov SA, Liu ZG (2004) Tumor necrosis factor-induced nonapoptotic cell death requires receptor-interacting protein-mediated cellular reactive oxygen species accumulation. J Biol Chem 279:10822–10828. doi:10.1074/jbc.M313141200
13. Cusson-Hermance N, Khurana S, Lee TH, Fitzgerald KA, Kelliher MA (2005) Rip1 mediates the Trif-dependent toll-like receptor 3- and 4-induced NF-kB activation but does not

contribute to interferon regulatory factor 3 activation. J Biol Chem 280:36560–36566. doi:10.1074/jbc.M506831200
14. Hsu H, Huang J, Shu HB, Baichwal V, Goeddel DV (1996) TNF dependent recruitment of the protein kinase RIP to the TNF receptor-1 signaling complex. Immunity 4:387–396. doi:10.1016/S1074-7613(00)80252-6
15. Meylan E, Burns K, Hofmann K, Blancheteau V, Martinon F, Kelliher M, Tschopp J (2004) RIP1 is an essential mediator of Toll-like receptor3-induced NF-kB activation. Nat Immunol 5:503–507. doi:10.1038/ni1061
16. Ting AT, Pimentel-Muinos FX, Seed B (1996) RIP mediates tumor necrosis factor receptor 1 activation of NF-kappaB but not Fas/APO-1-initiated apoptosis. EMBO J 15:6189–6196
17. Degterev A, Huang Z, Boyce M, Li Y, Jagtap P, Mizushima N, Cuny GD, Mitchison TJ, Moskowitz MA, Yuan J (2005) Chemical inhibitor of nonapoptotic cell death with therapeutic potential for ischemic brain injury. Nat Chem Biol 1:112–119. doi:10.1038/nchembio711
18. Degterev A, Hitomi J, Germscheid M, Ch'en IL, Korkina O, Teng X, Abbott D, Cuny GD, Yuan C, Wagner G, Hedrick SM, Gerber SA, Lugovskoy A, Yuan J (2008) Identification of RIP1 kinase as a specific cellular target of necrostatins. Nat Chem Biol 5:313–321. doi:10.1038/nchembio.83
19. Ch'en IL, Beisner DR, Degterev A, Lynch C, Yuan J, Hoffmann A, Hedrick SM (2008) Antigen-mediated T cell expansion regulated by parallel pathways of death. Proc Natl Acad Sci USA 105:17463–17468. doi:10.1073/pnas.0808043105
20. Smith CC, Davidson SM, Lim SY, Simpkin JC, Hothersall JS, Yellon DM (2007) Necrostatin: a potentially novel cardioprotective agent? Cardiovasc Drugs Ther 21:227–233. doi:10.1007/s10557-007-6035-1
21. Xu X, Chua CC, Kong J, Kostrzewa RM, Kumaraguru U, Hamdy RC, Chua BH (2007) Necrostatin-1 protects against glutamate-induced glutathione depletion and caspase-independent cell death in HT-22 cells. J Neurochem 103:2004–2014. doi:10.1111/j.1471-4159.2007.04884.x
22. Bao L, Li Y, Deng SX, Landry D, Tabas I (2006) Sitosterol-containing lipoproteins trigger free sterol-induced caspase-independent death in ACAT-competent macrophages. J Biol Chem 281:33635–33649. doi:10.1074/jbc.M606339200
23. Hong Q, Hsu LJ, Schultz L, Pratt N, Mattison J, Chang NS (2007) Zfra affects TNF-mediated cell death by interacting with death domain protein TRADD and negatively regulates the activation of NF-kappaB, JNK1, p53 and WOX1 during stress response. BMC Mol Biol 8:50. doi:10.1186/1471-2199-8-50
24. Declercq W, VandenBerghe T, Vandenabeele P (2009) RIP kinases at the crossroads of cell death and survival. Cell 23:229–232. doi:10.1016/j.cell.2009.07.006
25. Wermuth CG (2006) Pharmacophores: historical perspective and viewpoint from a medicinal chemist. In: Langer T, Hoffmann RD (eds) Pharmacophores and pharmacophore searches, 1st edn. Wiley, New York, pp 1–13
26. Ekins S, Mestres J, Testa B (2007) In silico pharmacology for drug discovery: methods for virtual ligand screening and profiling. Br J Pharmacol 152:9–20. doi:10.1038/sj.bjp.0707305
27. Nair SB, Fayaz SM, Krishnamurthy RG (2012) In silico prediction of novel inhibitors of the DNA binding activity of FoxG1. Med Chem 8:1155–1162. doi:10.2174/1573406411208061155
28. Yang SY (2010) Pharmacophore modeling and applications in drug discovery: challenges and recent advances. Drug Discov Today 15:444–450. doi:10.1016/j.drudis.2010.03.013
29. Dror O, Shulman-Peleg A, Nussinov R, Wolfson HJ (2004) Predicting molecular interactions in silico: I. A guide to pharmacophore identification and its applications to drug design. Curr Med Chem 11:71–90. doi:10.2174/0929867043456287
30. Khedkar SA, Malde AK, Coutinho EC, Srivastava S (2007) Pharmacophore modeling in drug discovery and development: an overview. Med Chem 3:187–197. doi:10.2174/157340607780059521
31. Wolber G, Seidel T, Bendix F, Langer T (2008) Molecule-pharmacophore superpositioning and pattern matching in computational drug design. Drug Discov Today 13:23–29. doi:10.1016/j.drudis.2007.09.007
32. Kirchmair J, Laggner C, Wolber G, Langer T (2005) Comparative analysis of protein-bound ligand conformations with respect to catalyst's conformational space subsampling algorithms. J Chem Inf Model 45:422–430. doi:10.1021/ci0497531
33. Kirchmair J, Wolber G, Laggner C, Langer T (2006) Comparative performance assessment of the conformational model generators omega and catalyst: a large-scale survey on the retrieval of protein-bound ligand conformations. J Chem Inf Model 46:1848–1861. doi:10.1021/ci060084g
34. Kristam R, Gillet VJ, Lewis RA, Thorner D (2005) Comparison of conformational analysis techniques to generate pharmacophore hypotheses using catalyst. J Chem Inf Model 45:461–476. doi:10.1021/ci049731z
35. Hecker EA, Duraiswami C, Andrea TA, Diller DJ (2002) Use of catalyst pharmacophore models for screening of large combinatorial libraries. J Chem Inf Comput Sci 42:1204–1211. doi:10.1021/ci020368a
36. Toba S, Srinivasan J, Maynard AJ, Sutter J (2006) Using pharmacophore models to gain insight into structural binding and virtual screening: an application study with CDK2 and human DHFR. J Chem Inf Model 46:728–735. doi:10.1021/ci050410c
37. Vadivelan S, Sinha BN, Irudayam SJ, Jagarlapudi SA (2007) Virtual screening studies to design potent CDK2-cyclin A inhibitors. J Chem Inf Model 47:1526–1535. doi:10.1021/ci7000742
38. Kurogi Y, Güner OF (2001) Pharmacophore modeling and three-dimensional database searching for drug design using catalyst. Curr Med Chem 8:1035–1055. doi:10.2174/0929867013372481
39. Güner OF (2002) History and evolution of the pharmacophore concept in computer-aided drug design. Curr Top Med Chem 2:1321–1332. doi:10.2174/1568026023392940
40. Xiao Z, Varma S, Xiao YD, Tropsha A (2004) Modeling of p38 mitogen-activated protein kinase inhibitors using the Catalyst HypoGen and k-nearest neighbor QSAR methods. J Mol Graph Model 23:129–138. doi:10.1016/j.jmgm.2004.05.001
41. Saxena S, Devi PB, Soni V, Yogeeswari P, Sriram D (2014) Identification of novel inhibitors against Mycobacterium tuberculosis L-alanine dehydrogenase (MTB-AlaDH) through structure-based virtual screening. J Mol Graph Model 47:37–43. doi:10.1016/j.jmgm.2013.08.005
42. Nair SB, Fayaz SM, Rajanikant GK (2013) A novel multi-target drug screening strategy directed against key proteins of DAPk family. Comb Chem High Throughput Screen 16:449–457. doi:10.2174/1386207311316060005
43. Zou J, Xie HZ, Yang SY, Chen JJ, Ren JX, Wei YQ (2008) Towards more accurate pharmacophore modeling: multicomplex based comprehensive pharmacophore map and most-frequent-feature pharmacophore model of CDK2. J Mol Graph Model 27:430–438. doi:10.1016/j.jmgm.2008.07.004
44. Hein M, Zilian D, Sotriffer CA (2010) Docking compared to 3D pharmacophores: the scoring function challenge. Drug Discov Today Technol 7:229–236. doi:10.1016/j.ddtec.2010.12.003
45. Drwal MN, Agama K, Pommier Y, Griffith R (2013) Development of purely structure-based pharmacophores for the topoisomerase I-DNA-ligand binding pocket. J Comput Aided Mol Des 27:1037–1049. doi:10.1007/s10822-013-9695-x
46. Thangapandian S, John S, Sakkiah S, Lee KW (2010) Docking-enabled pharmacophore model for histone deacetylase 8

inhibitors and its application in anti-cancer drug discovery. J Mol Graph Model 29:382–395. doi:10.1016/j.jmgm.2010.07.007
47. Friesner RA, Banks JL, Murphy RB, Halgren TA, Klicic JJ, Mainz DT, Repasky MP, Knoll EH, Shelley M, Perry JK, Shaw DE, Francis P, Shenkin PS (2004) Glide: a new approach for rapid, accurate docking and scoring. 1. Method and assessment of docking accuracy. J Med Chem 47:1739–1749. doi:10.1021/jm0306430
48. Salam NK, Nuti R, Sherman W (2009) Novel method for generating structure-based pharmacophores using energetic analysis. J Chem Inf Model 49:2356–2368. doi:10.1021/ci900212v
49. Irwin JJ, Shoichet BK (2005) ZINC—a free database of commercially available compounds for virtual screening. J Chem Inf Model 45:177–182. doi:10.1021/ci049714
50. Verdonk ML, Mortenson PN, Hall RJ, Hartshorn MJ, Murray CW (2008) Protein-ligand docking against non-native protein conformers. J Chem Inf Model 48:2214–2225. doi:10.1021/ci8002254
51. Cavasotto CN (2012) Normal mode-based approaches in receptor ensemble docking. Methods Mol Biol 819:157–168. doi:10.1007/978-1-61779-465-0_11
52. Laskowski RA, Swindells MB (2011) LigPlot + : multiple ligand-protein interaction diagrams for drug discovery. J Chem Inf Model 51:2778–2786. doi:10.1021/ci200227u
53. Van Der Spoel D, Lindahl E, Hess B, Groenhof G, Mark AE, Berendsen HJ (2005) GROMACS: fast, flexible, and free. J Comput Chem 26:1701–1718. doi:10.1002/jcc.20291
54. Hess B, Kutzner C, van der Spoel D, Lindahl E (2008) GROMACS 4: algorithms for highly efficient, load-balanced, and scalable molecular simulation. J Chem Theory Comput 4:435–447. doi:10.1021/ct700301q
55. Oostenbrink C, Villa A, Mark AE, van Gunsteren WF (2004) A biomolecular force field based on the free enthalpy of hydration and solvation: the GROMOS force-field parameter sets 53A5 and 53A6. J Comput Chem 25:1656–1676. doi:10.1002/jcc.20090
56. van Aalten DM, Bywater R, Findlay JB, Hendlich M, Hooft RW, Vriend G (1996) PRODRG, a program for generating molecular topologies and unique molecular descriptors from coordinates of small molecules. J Comput Aided Mol Des 10:255–262. doi:10.1007/BF00355047
57. Darden T, York D, Pedersen L (1993) Particle mesh Ewald—an N. log(N) method for Ewald sums in large systems. J Chem Phys 98:10089–10093. doi:10.1063/1.464397
58. Berendsen HJC, Postma JPM, Van Gunsteren WF, DiNola A, Haak JR (1984) Molecular dynamics with coupling to an external bath. J Chem Phys 81:3684–3691. doi:10.1063/1.448118
59. Humphrey W, Dalke A, Schulten K (1996) VMD: visual molecular dynamics. J Mol Graph 14:33–38
60. Degterev A, Hitomi J, Germscheid M, Ch'en IL, Korkina O, Teng X, Abbott D, Cuny GD, Yuan C, Wagner G, Hedrick SM, Gerber SA, Lugovskoy A, Yuan J (2008) Identification of RIP1 kinase as a specific cellular target of necrostatins. Nat Chem Biol 4:313–321. doi:10.1038/nchembio.83
61. Maki JL, Smith EE, Teng X, Ray SS, Cuny GD, Degterev A (2012) Fluorescence polarization assay for inhibitors of the kinase domain of receptor interacting protein 1. Anal Biochem 427:164–174. doi:10.1016/j.ab.2012.05.019
62. Xie T, Peng W, Liu Y, Yan C, Maki J, Degterev A, Yuan J, Shi Y (2013) Structural basis of RIP1 inhibition by necrostatins. Structure 21:493–499. doi:10.1016/j.str.2013.01.016
63. Wu Z, Li Y, Cai Y, Yuan J, Yuan C (2013) A novel necroptosis inhibitor-necrostatin-21 and its SAR study. Bioorg Med Chem Lett 23:4903–4906. doi:10.1016/j.bmcl.2013.06.073
64. Harris PA, Bandyopadhyay D, Berger SB, Campobasso N, Capriotti CA, Cox JA, Dare L, Finger JN, Hoffman SJ, Kahler KM, Lehr R, Lich JD, Rakesh N, Nolte RT, Ouellette MT, Pao CS, Schaeffer MC, Smallwood A, Sun HH, Swift BA, Totoritis RD, Ward P, Marquis RW, Bertin J, Gough PJ (2013) Discovery of small molecule RIP1 kinase inhibitors for the treatment of pathologies associated with necroptosis. ACS Med Chem Lett 4:1238–1243. doi:10.1021/ml400382p
65. Bender A, Glen RC (2005) A discussion of measures of enrichment in virtual screening: comparing the information content of descriptors with increasing levels of sophistication. J Chem Inf Model 45:1369–1375. doi:10.1021/ci0500177
66. Jain AN, Nicholls A (2008) Recommendations for evaluation of computational methods. J Comput Aided Mol Des 22:133–139. doi:10.1007/s10822-008-9196-5
67. Hamza A, Wei NN, Zhan CG (2012) Ligand-based virtual screening approach using a new scoring function. J Chem Inf Model 52:963–974. doi:10.1021/ci200617d